

# Ferroelectric switchable altermagnetism

Mingqiang Gu,<sup>1</sup> Yuntian Liu,<sup>1</sup> Haiyuan Zhu,<sup>1</sup> Kunihiro Yananose,<sup>2</sup> Xiaobing Chen,<sup>1</sup> Yongkang Hu,<sup>1</sup> Alessandro Stroppa,<sup>3,\*</sup> and Qihang Liu<sup>1,4,†</sup>

<sup>1</sup>*Department of Physics and Guangdong Basic Research Center of Excellence for Quantum Science, Southern University of Science and Technology, Shenzhen 518055, China*

<sup>2</sup>*Korea Institute for Advanced Study, Seoul 02455, Republic of Korea*

<sup>3</sup>*CNR-SPIN, c/o Dip.to di Scienze Fisiche e Chimiche - Università degli Studi dell'Aquila - Via Vetoio - 67100 - Coppito (AQ), Italy*

<sup>4</sup>*Guangdong Provincial Key Laboratory of Computational Science and Material Design, Southern University of Science and Technology, Shenzhen 518055, China*

(Dated: November 22, 2024)

We propose a novel ferroelectric switchable altermagnetism effect, the reversal of ferroelectric polarization is coupled to the switching of altermagnetic spin splitting. We demonstrate the design principles for the ferroelectric altermagnets and the additional symmetry constraints necessary for switching the altermagnetic spin splitting through flipping the electric polarization based on the state-of-the-art spin-group symmetry techniques. 22 ferroelectric altermagnets are found by screening through the 2001 experimental reported magnetic structures in the MAGNDATA database and 2 of them are identified as ferroelectric switchable altermagnets. Using the hybrid improper ferroelectric material  $[\text{C}(\text{NH}_2)_3]\text{Cr}(\text{HCOO})_3$  as an example, we show how the altermagnetic spin splitting is tightly coupled to the ferroelectric polarization, providing an ideal platform for designing electric-field-controllable multiferroic devices. Finally, we find that such manipulation of altermagnetism can be detected by monitoring the physical quantities that are related to the non-vanishing Berry curvature dipole, such as the linearly polarized photogalvanic spin current.

*Introduction* - Multiferroic materials exhibit more than one type of ferroic order simultaneously, such as ferroelectricity (spontaneous electric polarization) and magnetism (ferromagnetism or antiferromagnetism) [1]. In particular, magnetoelectrically coupled multiferroic materials have attracted significant interest due to their potential for controlling magnetic properties through electric fields, and vice versa, opening pathways for innovative applications in memory storage, sensors, and spintronics [2–5]. Multiferroics are broadly categorized into two types [6]. In type-I multiferroics, ferroelectric and magnetic orders originate from distinct mechanisms [7, 8], which often results in weak coupling between these order parameters. In contrast, type-II multiferroics demonstrate stronger coupling because ferroelectricity arises directly from magnetic ordering [9]. Historically, the design and manipulation of multiferroicity primarily rely on the interaction between net magnetic moments and electric polarization [10]. For example, in multiferroic antiferromagnet  $\text{Ca}_3\text{Mn}_2\text{O}_7$ , the multiferroic coupling stems from the ferroelectric polarization and the net magnetic moment induced by spin-orbit coupling (SOC), i.e., Dzyaloshinskii–Moriya interaction [11]. However, the small weak FM magnetization ( $0.045 \mu_B/\text{Mn}$  in theory and  $0.0025 \mu_B/\text{Mn}$  in experiment) [12] limits the strength of magnetoelectric coupling and thus the multiferroic applications.

Recently, altermagnetism [13, 14] has garnered considerable attention as a promising avenue for achieving novel spintronic properties. Altermagnets are a class of collinear antiferromagnetic (AFM) materials characterized by alternating spin polarization across recipro-

cal space due to breaking of certain spatial symmetries, even though they have no net macroscopic magnetization. The order parameter  $S$  featuring altermagnetism can be represented by the energy splitting between the two spin channels in certain paths of the Brillouin zone  $\Delta E_k^s = E_k^\uparrow - E_k^\downarrow$ . The spin-split bands of Bloch electrons in altermagnets create the possibility of designing new types of spintronic devices, e.g., spin-filtering magnetic tunnel junctions [15, 16]. Due to the combination of the advantages of FM and AFM in terms of spin splitting, altermagnetism is also considered a third type of collinear magnetism [13, 17].

In this *Letter*, we introduce the *ferroelectric switchable altermagnets*, a new class of materials which shows not only the coexistence of ferroelectricity and altermagnetism, but also the synergistic coupling of the two order parameters, leading to a reversal of spin-character in the splitted energy bands by switching the ferroelectric polarization. As illustrated in Fig. 1(a), in specific circumstances, the altermagnetic spin degree of freedom is tightly correlated to the electric polarization, indicating a distinct form of magnetoelectric coupling. Such a mechanism enables the control of a nonvolatile spin-split electronic dispersion through the external electric field, providing an efficient route to achieve robust all-in-one multiferroic memory devices. For example, Fig. 1(b) illustrates an electric-field-controllable spin-filtering altermagnetic tunnel junction device *without the need of switching the Néel vector*. By considering whether the spin-polarized Fermi surface between the sample and the substrate match or not [13], the resistance can be switched between high and low by simply switching the

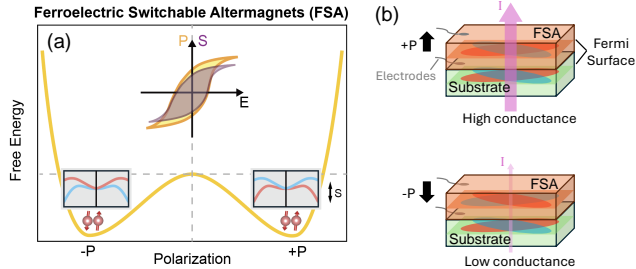


FIG. 1. (a) Schematic illustration of ferroelectric switchable altermagnets, where the altermagnetic spin splitting  $S$  strongly couples to the ferroelectric polarization  $P$ . (b) A non-volatile spin filtering tunnel junction device design with ferroelectric switchable altermagnets.

ferroelectric polarization. By applying the state-of-the-art spin-group symmetry analyses, we searched through all the MAGNDATA database [18] and screened 22 *ferroelectric altermagnets*, in which only two candidates support the synergistic switching of altermagnetic spin splitting through ferroelectric polarization.

In order to discuss a representative case of the ferroelectric switchable altermagnets, we perform first-principles calculations on the metal-organic framework (MOF) system  $[\text{C}(\text{NH}_2)_3]\text{Cr}(\text{HCOO})_3$ , which we will denote as Cr-MOF hereafter. This compound is isostructural to Cu-MOF found in MAGNDATA and is particularly interesting since it expands the search for potentially interesting altermagnets to the extremely tunable and versatile class of hybrid organic-inorganic perovskites for functional materials design. Cr-MOF has been experimentally synthesized, and it has been proposed as hybrid improper ferroelectric [19, 20]. Here, we predict that the altermagnetic spin splitting in this material is tightly coupled to the ferroelectric polarization, in both the magnitude and the sign of  $\Delta E_k^S$ , providing an ideal platform for designing electric-field-controllable spintronic devices. Finally, we find that the manipulation of altermagnetism can be monitored by the nonlinear optical generation of spin current, which originates from the non-zero Berry curvature dipole.

*Material design principles* - Altermagnetic spin splitting is a non-relativistic property that manifests without the need for spin-orbit coupling (SOC), where the symmetry-theoretical framework should adopt spin space group (SSG) [14, 21–25] instead of the commonly used magnetic space group (MSG). We first consider ferroelectric altermagnets where the two order parameters  $P$  and  $S$  are not necessarily coupled. Two rules under the framework of SSG emerge: i) For a collinear antiferromagnet manifesting spin splitting in the momentum space, the symmetries of joint parity and time-reversal ( $\mathcal{PT}$ ) and  $\mathcal{T}\tau$  with  $\tau$  being the fractional lattice translation, should

be broken; ii) For ferroelectric material, the spatial part of the parent space group (SG) of the SSG should belong to a polar group.

We diagnosed the SSGs of the 2001 experimentally reported magnetic structures in the MAGNDATA database by using our homemade online program FINDSPIN-GROUP [26], and found 22 systems that meet the above criteria. One immediately finds that the filtered materials can be divided into two classes by examining the MSG of the materials: the MSG of the first class allows weak spin canting, leading to a non-zero residual ferromagnetic (FM) moment, while the second class forbids net magnetic moment in the system. For the first class with  $P$ - $M$  coupling, the electronic polarization can interplay with the weak FM moment, leading to a classical magnetoelectric coupling [11]. Note that SOC plays an essential role (e.g., Dzyaloshinskii-Moriya interaction) in slightly tilting the spins from the collinear AFM configuration. For the second class without  $P$ - $M$  coupling, since the net magnetic moment is forbidden by MSGs, the flipping of electric polarization is not supposed to induce any macroscopic effect on the magnetization. However, both two classes are potential candidates for ferroelectric switchable altermagnets if the real-space electric polarization and the momentum-space spin splitting are coupled, even without SOC.

In general, the coexistence of electric polarization  $P$  and altermagnetic spin splitting  $\Delta E_k^S$  (denoted by  $S$ ) does not guarantee their coupling. Therefore, we next focus on the search of symmetry operations that synergistically switch  $P$  and  $S$ , and if these operations correspond to reasonable flipping paths under an external electric field, which does not change the Néel order. For example, considering an initial state  $\psi_k^i(P, S)$ , one can always flip both electric and spin polarization by applying a joint operation  $\mathcal{PT}$  to the system to get a reversed state  $\mathcal{PT}\psi_k^i(P, S) = \psi_k^f(-P, -S)$ . However, in the transition path connecting  $\psi_k^f(-P, -S)$  and  $\psi_k^i(P, S)$  phases, the Néel vector may also be reversed, indicating a transition path that cannot be achieved by electric field only. By going through the list in TABLE SI in Supplementary Materials, we found that the sign of  $\Delta E_k^S$  for most candidates remains unchanged during the polarization reversal, as exemplified by  $\text{PbNiO}_3$  in Supplementary Materials. Interestingly, there are two hybrid improper ferroelectric materials,  $\text{Ca}_3\text{Mn}_2\text{O}_7$  and  $[\text{C}(\text{NH}_2)_3]\text{Cr}(\text{HCOO})_3$ , as prototypical candidates of ferroelectric switchable altermagnets.

*Altermagnetism in hybrid improper ferroelectric Cr-MOF* - Hybrid improper ferroelectricity arises from a combination of two or more lattice modes that individually preserve inversion symmetry but collectively breaks it, resulting in a spontaneous polarization. Several candidate materials from Class 1 in TABLE SI belong to this category, including  $\text{Ca}_3\text{Mn}_2\text{O}_7$  (SG  $Cmc2_1$ ) [27] and the hybrid organic-inorganic per-

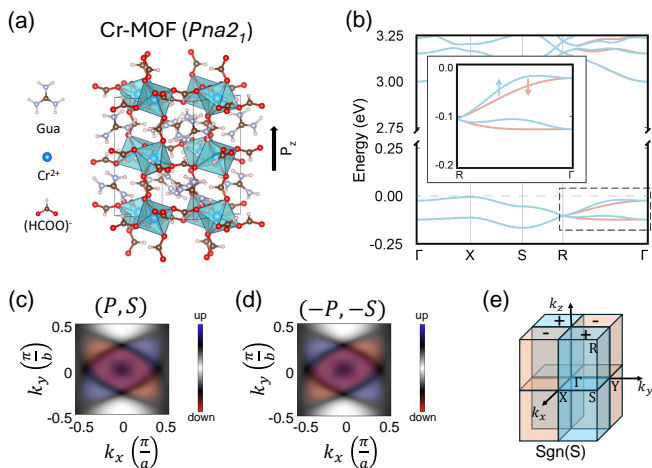


FIG. 2. (a) Crystal structure of Cr-MOF. (b) Spin-split band structure of Cr-MOF. (c) Spin-resolved isoenergy contour ( $E = -0.05$  eV) for the  $(P, S)$  state at the  $k_z = 0.25$  plane, blue and red denote the spectral weight for spin up and spin down, respectively. (d) Same as (c), but for the  $(-P, -S)$  state. (e) The sign of  $\Delta E_k^S$  for the VBM in reciprocal space.

ovskite  $[\text{C}(\text{NH}_2)_3\text{M}(\text{HCOO})_3]$  (SG  $Pna2_1$ ) with M being transition-metal elements Cu or Cr. Below we use Cr-MOF (see Fig. 2(a)) to illustrate the design principles of ferroelectric switchable altermagnets for two reasons: (a) it exhibits the largest spin splitting near the Fermi level among this material family, and (b) various AFM configurations can be realized in Cr-MOF through compressive strain, offering an additional degree of freedom for phase manipulation [28]. Moreover, the compositional tunability in this family offers more flexibility in designing materials for spin-splitting magnitude optimization. While A-, C- and G-type AFM Cr-MOF are all altermagnets, here we focus on the C-type configuration, as it manifests the largest spin splitting near the Fermi level. Further discussions on other MOFs and AFM configurations can be found in the Supplementary Materials.

The spin-polarized band structure obtained from density functional theory (DFT) calculations is shown in Fig. 2(b). The band gap is about 3 eV, ensuring a good insulating background that is favorable for ferroelectrics. Notably, a large spin splitting is observed at the valence band maximum (VBM), with the largest energy difference being approximately 20 meV. Such spin splitting occurs at the relatively low-symmetry points in reciprocal space, such as along the  $\Gamma(0, 0, 0) \rightarrow R(0.5, 0.5, 0.5)$  path. The spin-polarized isoenergy contour at  $E = -0.05$  eV is shown in Fig. 2(c), showing a deviated feature compared with the so-called “d-wave” altermagnetism because of the absence of four-fold symmetry. Furthermore, the sign of  $\Delta E_k^S$ , as well as the spin polarization of a given spin-polarized band, are odd under mirror operations  $\{1||m_{100}\}$  and  $\{1||m_{010}\}$ , and even under  $\{1||m_{001}\}$ ,

as illustrated in Fig. 2(e).

*Synergistically switch of electric and spin polarizations* - Here, a state with the coexistence of polarization  $P$  ( $P//z$ ) and altermagnetism  $S$  is denoted as the  $(P, S)$  state. The SSG operations that map  $P \rightarrow -P$  and  $S \rightarrow -S$  are analyzed and listed in Fig. S3. While the SSG operations connecting  $P$  state to  $-P$  state can be one of the following:  $\{1||-1\}$ ,  $\{1||2_{100}\}$ ,  $\{1||2_{010}\}$ ,  $\{-1||-1\}$ ,  $\{-1||2_{100}\}$ , and  $\{-1||2_{010}\}$ , only three of them map the  $(P, S)$  state to the  $(-P, -S)$  state, i.e.,  $\{1||2_{100}\}$ ,  $\{1||2_{010}\}$ , and  $\{-1||-1\}$ . In addition, whether the  $(-P, -S)$  state can be experimentally realized upon the application of an electric field, however, depends on the energy barrier between the two phases, which is ultimately governed by the internal atomic displacements during the phase transition.

The search for the reversed polarization state can also be achieved by considering the mode decomposition of hybrid improper ferroelectricity. The electric polarization of Cr-MOF along the  $z$  direction is activated by two non-polar lattice distortion modes through a trilinear coupling  $F = \gamma Q_{X_1^-} Q_{X_4^+} Q_P$ , where  $Q_{X_1^-}$ ,  $Q_{X_4^+}$  and  $Q_P$  represent the amplitudes of the two zone-boundary non-polar distortion modes and the polar distortion mode, respectively, relative to the high symmetry  $Imma$  phase [19]. Reversing either of the zone-boundary modes flips the polarization  $P \rightarrow -P$ , while, reversing both, preserves  $P$ . As shown in Fig. 3(a), the  $X_1^-$  mode consist of two major distortions: a “scissor”-like distortion for the equatorial Cr-O bonds and a rotation of the guanidinium molecule by about  $42^\circ$ . The  $X_4^+$  mode corresponds primarily to a  $Q_2$  Jahn-Teller (JT) distortion of the Cr octahedra, with minimal impact on the organic molecules. Starting from the  $Imma$  structure, imposing only the  $X_1^-$  ( $X_4^+$ ) mode results in a centrosymmetric  $Pnna$  ( $Pnma$ ) structure. The combination of both  $X_1^-$  and  $X_4^+$  modes leads to the  $Pna2_1$  structure, a polar SG that induces the softening of the polar distortion. Since the polar distortion is a secondary effect arising from the coupling of the zone-boundary modes, the interplay between these two modes fully determines the final structure and its related properties in this system. For simplicity, and without loss of generality, we will use these two unstable modes ( $X_1^-$  and  $X_4^+$ ) as variables in the discussion below.

Fig. 3(b) shows the energy landscape of the coupled zone-boundary modes relative to the  $Imma$  phase. Starting from the energetically favored  $(P, S)$  ground state, if the amplitude of  $X_1^-$  mode is continuously reduced and eventually reversed its sign, the structure transforms to a  $(-P, S)$  state. This transition path, indicated by the purple line in Fig. 3(b), passes through a centrosymmetric  $Pnma$  phase. The  $(-P, S)$  state and the original  $(P, S)$  state are related by  $\{1||m_{001}\}$  SSG operation. The energy barrier is about 4 eV per unit cell, as shown in the left panel of Fig. 3(c). Such a high energy barrier is attributed to the large atomic distortion amplitude ( $\sim 6.3$

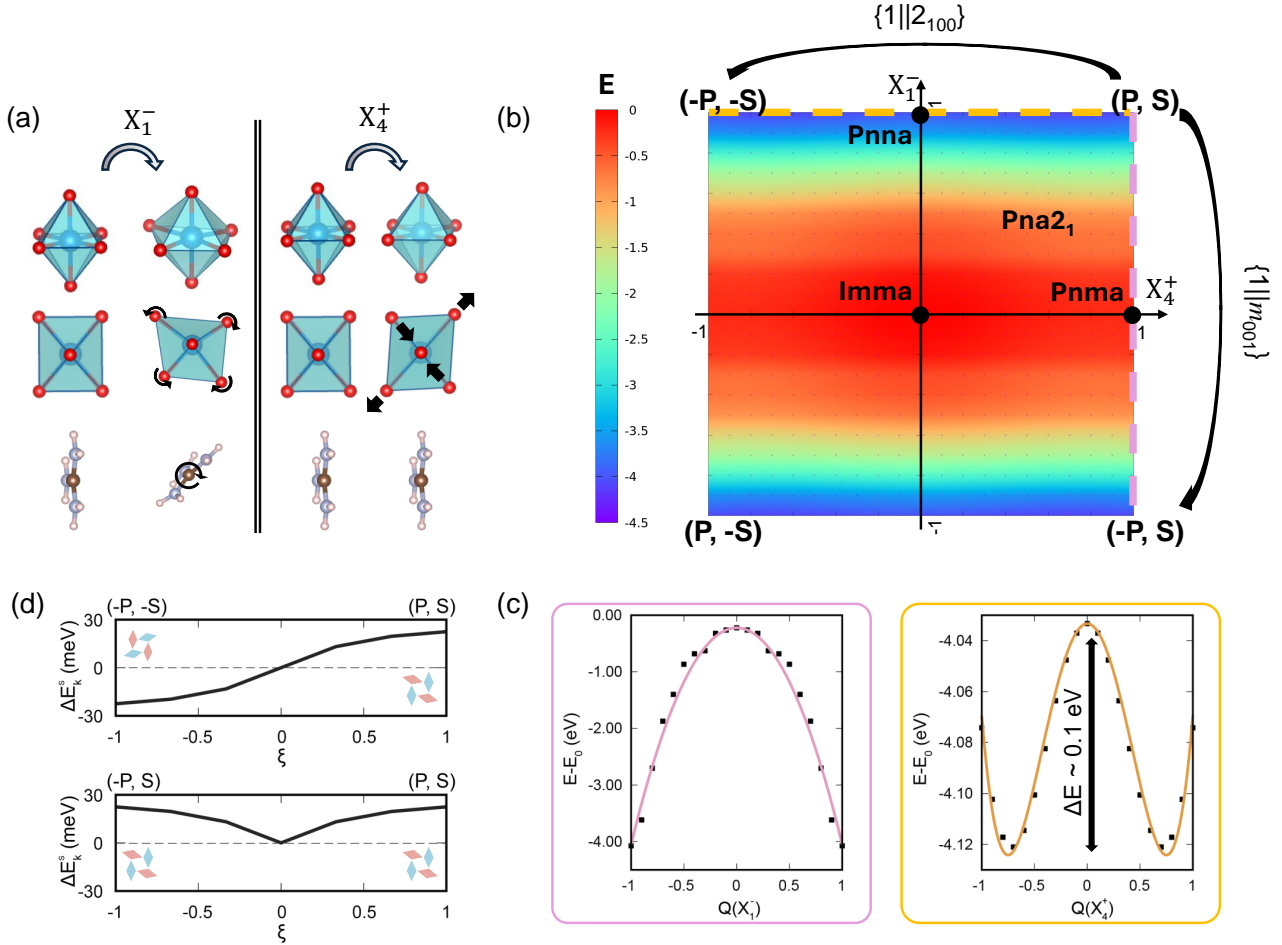


FIG. 3. (a) The hybrid improper coupled zone-boundary distortion modes in Cr-MOF. (b) Energy landscape for the coupling of the  $X_1^-$  and  $X_4^+$  modes, where different transition paths are marked by yellow and purple dashed lines. (c) Energy profiles along the two paths denoted in (b). (d) Spin splitting as a function of the interpolation structural parameter  $\xi$ . The insets in (d) denote the  $Q_2$  JT pattern at the endpoints, with the pink and blue diamonds denote the octahedra centered with the spin-up and spin-down Cr, respectively. The elongated octahedra form an antiferro-distortive JT distortion pattern associated to the orbital-ordering which “pseudo-rotate” from the two endpoints  $(P, S)$  and  $(-P, -S)$ .

Å) along this path, primarily due to the rotation of the guanidinium molecule. In sharp contrast, when the  $X_4^+$  mode is continuously tuned to the reversed amplitude, the transition occurs via a  $Pnna$  reference phase (orange line in Fig. 3(b)). This path leads to the  $(-P, -S)$  state, connected by  $\{1||2_{100}\}$  SSG operation, with a significantly lower energy barrier of approximately 0.1 eV (the right panel of Fig. 3(c)), nearly 40-times smaller than that for the  $Pnma$  path. Thus, the  $(P, S) \rightarrow (-P, -S)$  structural transition through the  $Pnna$  path is energetically favored and represents a possible realistic transition pathway when polar direction is flipped by an external electric field.

The spin reversal of the isoenergy contour for the  $(-P, -S)$  state shown in Fig. 2(d) strongly supports the possibility to control altermagnetic spin splitting by flipping the ferroelectric polarization in this system. To quantify this transition, we define a normalized inter-

polating structural parameter  $\xi$ , where  $\xi = 1$  represents the  $(P, S)$  structure and  $\xi = -1$  corresponds to either the  $(-P, S)$  or  $(-P, -S)$  structure. The evolution of  $\Delta E_k^s$  during the structural transition is plotted in Fig. 3(d). We found that  $\Delta E_k^s$  changes monotonically during the  $(P, S) \rightarrow (-P, -S)$  transition, while in the  $(P, S) \rightarrow (-P, S)$  transition it reduces to zero at the  $Pnma$  phase and then regresses to its original value. Such behavior arises because  $\Delta E_k^s$  is odd under  $\{1||2_{100}\}$  but even under  $\{1||m_{001}\}$ , consistent with the symmetry presented in Fig. 2(e). Furthermore, the microscopic mechanism of the reversal of the altermagnetic spin splitting by reversing the  $X_4^+$  mode can be understood by the change of the  $Q_2$  JT distortion pattern, as illustrated in the insets of Fig. 3(d). Since the JT distortion is known to couple with the orbital ordering in oxide perovskites [29] and MOF systems [30], our results provide a concrete example of how altermagnetism can be entangled

with orbital ordering [31], offering new insights into the control of spin splitting through orbital as well as lattice degrees of freedoms.

*Detection of the switch of altermagnetic spin splitting* - The direct experimental detection of the AFM-induced spin splitting typically requires advanced techniques such as spin-resolved angle-resolved photoemission spectroscopy [32, 33]. Since the Néel vector remains unchanged through  $(P, S) \rightarrow (-P, -S)$  transition, we propose a way to detect the switch of altermagnetic spin splitting through the linear-polarized photogalvanic spin current effect (spin LPGE), which directly couples to the spin polarization through nonlinear optical response. By using the SSG symmetry analysis implemented in FINDSPINGROUP, we find that six non-zero Berry curvature dipole (BCD) tensor elements ( $D_{xxz}, D_{xzx}, D_{zxx}, D_{yyz}, D_{yzy}, D_{zzy}$ ) are allowed without SOC in Cr-MOF. All the other tensor elements, such as the quantum metric dipole and inverse mass dipole [34], are forbidden. The non-zero BCD can induce a nonlinear Hall current in transport measurement, as well as the spin LPGE from an optical perspective. Due to the broken spatial inversion symmetry, a shift current is expected under linear-polarized light excitation [35]. In Cr-MOF system, both charge and spin currents can be generated: the charge current reflects the direction of the electric polarization  $P$ , while the spin current serves as a signature of the difference between the two spin channels, i.e. the spin splitting.

The spin LPGE conductivity component  $\sigma_{\uparrow\downarrow}^{zy}$  for the  $(P, S)$  and  $(-P, -S)$  states is shown in Fig. 4. A non-zero dc current begins to emerge when the photon energy exceeds the band gap, reaching the first peak at about 3.2 eV with a value of about  $0.23 \mu A/V^2$ . The second peak, near 4 eV, is attributed to the spin splitting at the higher conduction bands. During the  $(P, S) \rightarrow (-P, -S)$  structure transition, the sign of the spin LPGE current reverses. Therefore, the spin LPGE current can serve as a signature of the reversal of the altermagnetic spin splitting.

*Conclusion and discussion* - Recently, the gate-field control of different spin channels in a layered altermagnet through spin-valley-layer locking effect has been proposed [36], highlighting the importance for the manipulation of spin degree of freedom in altermagnets. However, such a non-versatile strategy requires the constant application of an external electric field, which is not favorable for storage devices unless further integration with other materials. On the other hand, sliding ferroelectricity can also be used to tune the  $\mathcal{PT}$  symmetry in a complex van der Waals sandwich heterojunction systems [37], which eventually controls emergence of the altermagnetic state. However, it requires an intrinsic AFM monolayer system in the center of the heterojunction, which is somehow rare. Considering that the hybrid improper ferroelectric materials can be artificially designed by chemistry or

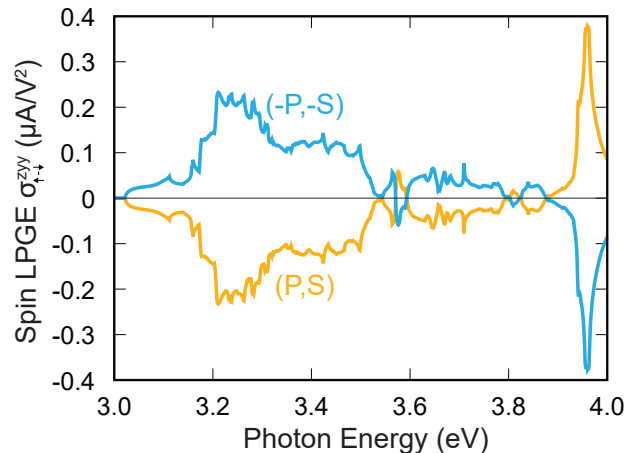


FIG. 4. The spin LPGE conductivity component  $\sigma_{\uparrow\downarrow}^{zy}$  for the  $(P, S)$  and  $(-P, -S)$  states.

strain engineering [38], our study provides a wide configuration space for designing versatile ferroelectric switchable altermagnets.

Our approach provides a novel method for controlling spin properties through ferroelectric polarization, which differs from traditional magnetoelectric multiferroics where ferroelectricity is used to control the net magnetic moment. For class 1 candidates, such as  $\text{Ca}_3\text{Mn}_2\text{O}_7$ , both approaches can work synergistically, offering multiple degrees of freedom for material manipulation. The coupling of electric polarization to both the weak FM moment and spin splitting provides enhanced versatility in device design. In contrast, for class 2 candidates where there is no net magnetic moment and most traditional magnetic detection method such as magneto-optical Kerr effect [39] would be ineffective, our approach still offers a viable pathway to achieve magnetoelectric coupling by correlating the electric polarization with spin splitting in reciprocal space. To conclude, ferroelectric switchable altermagnetism is a new type of magnetoelectric coupling beyond what is achievable in traditional multiferroics based solely on the spin-orbit interaction, paving an new functional materials platform for designing all-electric-controlled spintronic devices.

A.S. thanks useful discussions with P. Radaelli (Oxford University), P. Barone (CNR-SPIN), Sang-Wook Cheong (Rutgers University) and Xinfeng Chen (Xi'an Jiaotong University). This work was supported by the National Key R&D Program of China under Grant No. 2019YFA0704900, the National Natural Science Foundation of China under Grant No. 12274194, Guangdong Provincial Key Laboratory for Computational Science and Material Design under Grant No. 2019B030301001, Shenzhen Science and Technology Program (Grants No. RCJC20221008092722009

and No. 20231117091158001), the Innovative Team of General Higher Educational Institutes in Guangdong Province (Grant No. 2020KCXTD001), Guangdong Provincial Quantum Science Strategic Initiative under Grant No. GDZX2401002, the Science Technology and Innovation Commission of Shenzhen Municipality (JCYJ20210324104812034), Natural Science Foundation of Guangdong Province (2021A1515110389) and Center for Computational Science and Engineering of Southern University of Science and Technology. This work has been funded by the European Union - NextGenerationEU, Mission 4, Component 1, under the Italian Ministry of University and Research (MUR) National Innovation Ecosystem grant ECS00000041-VITALITY-CUP B43C22000470005. We also acknowledge the support by bilateral agreement for scientific collaboration CNR and NSFC (China), "Ferroelectric and chiral hybrid organic inorganic perovskites", for the years 2024-2025 (CUP B53C2300716000). K.Y. was supported by an individual grant (No. CG092501) at Korea Institute for Advanced Study.

---

\* alessandro.stroppa@spin.cnr.it

† liuqh@sustech.edu.cn

- [1] H. Schmid, *Ferroelectrics* **162**, 317 (1994).
- [2] N. A. Spaldin, *MRS Bulletin* **42**, 385 (2017).
- [3] R. Ramesh and N. A. Spaldin, *Nat Mater* **6**, 21 (2007).
- [4] M. Fiebig, T. Lottermoser, D. Meier, and M. Trassin, *Nature Reviews Materials* **1**, 16046 (2016).
- [5] X.-Z. Lu and J. M. Rondinelli, *Handbook of Materials Modeling: Applications: Current and Emerging Materials*, 1151 (2020).
- [6] D. Khomskii, *Physics* **2**, 20 (2009).
- [7] J. Wang, J. B. Neaton, H. Zheng, V. Nagarajan, S. B. Ogale, B. Liu, D. Viehland, V. Vaithyanathan, D. G. Schlom, U. V. Waghmare, N. A. Spaldin, K. M. Rabe, M. Wuttig, and R. Ramesh, *Science* **299**, 1719 (2003).
- [8] B. B. Van Aken, T. T. M. Palstra, A. Filippetti, and N. A. Spaldin, *Nature Materials* **3**, 164 (2004).
- [9] T. Kimura, T. Goto, H. Shintani, K. Ishizaka, T. Arima, and Y. Tokura, *Nature* **426**, 55 (2003).
- [10] M. Mostovoy, *npj Spintronics* **2**, 18 (2024).
- [11] N. A. Benedek and C. J. Fennie, *Physical Review Letters* **106**, 107204 (2011).
- [12] M. Liu, Y. Zhang, L.-F. Lin, L. Lin, S. Yang, X. Li, Y. Wang, S. Li, Z. Yan, X. Wang, X.-G. Li, S. Dong, and J.-M. Liu, *Applied Physics Letters* **113**, 022902 (2018).
- [13] L. Šmejkal, J. Sinova, and T. Jungwirth, *Physical Review X* **12**, 040501 (2022).
- [14] L. Šmejkal, J. Sinova, and T. Jungwirth, *Physical Review X* **12**, 031042 (2022).
- [15] K. Samanta, D.-F. Shao, and E. Y. Tsybal, *arXiv e-prints*, arXiv:2409.00195 (2024).
- [16] B. Chi, L. Jiang, Y. Zhu, G. Yu, C. Wan, and X. Han, *arXiv e-prints*, arXiv:2409.03415 (2024).
- [17] L. Bai, W. Feng, S. Liu, L. Šmejkal, Y. Mokrousov, and Y. Yao, *Advanced Functional Materials*, 2409327 (2024).
- [18] S. V. Gallego, J. M. Perez-Mato, L. Elcoro, E. S. Tasci, R. M. Hanson, K. Momma, M. I. Aroyo, and G. Madariaga, *Journal of Applied Crystallography* **49**, 1750 (2016).
- [19] A. Stroppa, P. Barone, P. Jain, J. M. Perez-Mato, and S. Picozzi, *Advanced Materials* **25**, 2284 (2013).
- [20] K. Yananose, E. R. Clark, P. J. Saines, P. Barone, A. Stroppa, and J. Yu, *Inorganic Chemistry* **62**, 17299 (2023).
- [21] P. Liu, J. Li, J. Han, X. Wan, and Q. Liu, *Physical Review X* **12**, 021016 (2022).
- [22] X. Chen, J. Ren, Y. Zhu, Y. Yu, A. Zhang, P. Liu, J. Li, Y. Liu, C. Li, and Q. Liu, *Physical Review X* **14**, 031038 (2024).
- [23] Y. Jiang, Z. Song, T. Zhu, Z. Fang, H. Weng, Z.-X. Liu, J. Yang, and C. Fang, *Physical Review X* **14**, 031039 (2024).
- [24] Z. Xiao, J. Zhao, Y. Li, R. Shindou, and Z.-D. Song, *Physical Review X* **14**, 031037 (2024).
- [25] X. Chen, Y. Liu, P. Liu, Y. Yu, J. Ren, J. Li, A. Zhang, and Q. Liu, *arXiv e-prints*, arXiv:2307.12366 (2023).
- [26] <https://www.findspingroup.com/>.
- [27] Y. Guo, H. Liu, O. Janson, I. C. Fulga, J. van den Brink, and J. I. Facio, *Materials Today Physics* **32**, 100991 (2023).
- [28] S. Ghosh, D. Di Sante, and A. Stroppa, *The Journal of Physical Chemistry Letters* **6**, 4553 (2015).
- [29] D. Khomskii, Cooperative Jahn–teller effect and orbital ordering, in *Transition Metal Compounds*, edited by D. I. Khomskii (Cambridge University Press, Cambridge, 2014) pp. 204–237.
- [30] A. Stroppa, P. Jain, P. Barone, M. Marsman, J. M. Perez-Mato, A. K. Cheetham, H. W. Kroto, and S. Picozzi, *Angewandte Chemie International Edition* **50**, 5847 (2011).
- [31] V. Leeb, A. Mook, L. Šmejkal, and J. Knolle, *Physical Review Letters* **132**, 236701 (2024).
- [32] J. Krempaský, L. Šmejkal, S. W. D'Souza, M. Hajaoui, G. Springholz, K. Uhlířová, F. Alarab, P. C. Constantinou, V. Strocov, D. Usanov, W. R. Pudelko, R. González-Hernández, A. Birk Hellenes, Z. Jansa, H. Reichlová, Z. Šobáň, R. D. Gonzalez Betancourt, P. Wadley, J. Sinova, D. Kriegner, J. Minár, J. H. Dil, and T. Jungwirth, *Nature* **626**, 517 (2024).
- [33] Y.-P. Zhu, X. Chen, X.-R. Liu, Y. Liu, P. Liu, H. Zha, G. Qu, C. Hong, J. Li, Z. Jiang, X.-M. Ma, Y.-J. Hao, M.-Y. Zhu, W. Liu, M. Zeng, S. Jayaram, M. Lenger, J. Ding, S. Mo, K. Tanaka, M. Arita, Z. Liu, M. Ye, D. Shen, J. Wrachtrup, Y. Huang, R.-H. He, S. Qiao, Q. Liu, and C. Liu, *Nature* **626**, 523 (2024).
- [34] H. Zhu, J. Li, X. Chen, Y. Yu, and Q. Liu, *arXiv e-prints*, arXiv:2406.03738 (2024).
- [35] M. S. Okyay, S. A. Sato, K. W. Kim, B. Yan, H. Jin, and N. Park, *Communications Physics* **5**, 303 (2022).
- [36] R.-W. Zhang, C. Cui, R. Li, J. Duan, L. Li, Z.-M. Yu, and Y. Yao, *Physical Review Letters* **133**, 056401 (2024).
- [37] W. Sun, W. Wang, C. Yang, R. Hu, S. Yan, S. Huang, and Z. Cheng, *Nano Letters* **24**, 11179 (2024).
- [38] D. Puggioni and J. M. Rondinelli, *Nature Communications* **5**, 3432 (2014).
- [39] F.-R. Fan, H. Wu, D. Nabok, S. Hu, W. Ren, C. Draxl, and A. Stroppa, *Journal of the American Chemical Society* **139**, 12883 (2017).